Vishal Tandon[1]
Sharath K. Bhagavatula[2]
Wyatt C. Nelson[3]
Brian J. Kirby[3]

[1]Department of Biomedical Engineering, Cornell University, Ithaca, NY, USA
[2]School of Electrical and Computer Engineering, Cornell University, Ithaca, NY, USA
[3]Sibley School of Mechanical and Aerospace Engineering, Cornell University, Ithaca, NY, USA

Received October 2, 2007
Revised December 5, 2007
Accepted December 5, 2007

Zeta potential and electroosmotic mobility in microfluidic devices fabricated from hydrophobic polymers: 1. The origins of charge

This paper combines new experimental data for electrokinetic characterization of hydrophobic polymers with a detailed discussion of the putative origins of charge at water-hydrophobe interfaces. Complexities in determining the origin of charge are discussed in the context of design and modeling challenges for electrokinetic actuation in hydrophobic microfluidic devices with aqueous working fluids. Measurements of interfacial charge are complicated by slip and interfacial water structuring phenomena (see Part 2, this issue). Despite these complexities, it is shown that (i) several hydrophobic materials, such as Teflon and Zeonor, have predictable electrokinetic properties and (ii) electrokinetic data for hydrophobic microfluidic systems is most consistent with the postulate that hydroxyl ion adsorption is the origin of charge.

Keywords:
Electroosmosis / Hydrophobic / Streaming potential / Surface charge / Zeta potential
DOI 10.1002/elps.200700734

1 Introduction

Polymers are attractive as microfluidic substrates owing to their biocompatibility, relatively low cost, ease of fabrication, and potential for both high chemical resistance and favorable optical properties [2–5]. Many commonly used polymers are hydrophobic, however, and electrokinetic actuation in hydrophobic microfluidic devices is not well-characterized owing to uncertainties in the chemistry of water-hydrophobe interfaces. This limits repeatability of experiments, accuracy of predictive models, and ultimately device design capabilities. Electrokinetic measurements in hydrophobic substrates are challenging (as evidenced by significant scatter in the data [6]) because these phenomena are difficult to measure and are sensitive to surfactants; theoretical models are also lacking because the physics of interfacial phenomena and the space of applicable input parameters are not well-defined. Most hydrophobic polymers do not have reactive surface groups or a strong affinity for ions, but often exhibit electrokinetic potentials on the same order as charged hydrophilic surfaces (such as glass), and have similar pH-dependence. In both hydrophilic and hydrophobic surfaces, accurate prediction of the electrokinetic potential depends on the veracity of models for both (i) interfacial charge formation, and (ii) diffuse and condensed ion distributions. For hydrophobic surfaces in particular, these models are further complicated in that the origins of charge are less well-understood, and electrokinetic potentials inferred from experiments may be inflated due to hydrodynamic slip [1, 7]. Despite the complexity of hydrophobic microfluidic systems, the fact that measurements of material properties inferred from electrokinetics experiments in varied systems are reproducible suggests that modeling electrokinetic behavior is possible through careful consideration of slip, surface chemistry, and surface morphology. In the sections to follow, we present general fundamental electrokinetic relations and then discuss the distinctive challenges in understanding the origins of interfacial charge in hydrophobic microfluidic materials. In the companion to this paper [1], we present slip phenomena and interfacial molecular/supramolecular structures, and show that they are inherently coupled with surface charge. Here we focus on microfluidic devices with aqueous electrolyte solutions, and exclude discussion of large amphipathic and organic surfactants.

Correspondence: Dr. Brian J. Kirby, 238 Upson Hall, Cornell University Ithaca, NY 14853, USA
E-mail: BK88@cornell.edu
Fax: +607-255-1222

Abbreviations: **ATR-IR**, attenuated total reflection infrared; **EDL**, electrical double layer; **MD**, molecular dynamics; **PDFP**, plasma deposited fluoropolymer; **PE**, polyethylene; **PS**, polystyrene; **pzc**, point of zero charge; **SFG**, sum frequency generation; **SHG**, second harmonic generation; **XPS**, X-ray photoelectron spectroscopy

2 Fundamentals of electrokinetics

Before we discuss the challenges that arise in characterizing hydrophobic microfluidic devices, we present a brief summary of the physical processes underlying electrokinetics in microfluidic systems in general.

2.1 Origins of surface charge

The spontaneous separation of charge at solid-liquid interfaces is ubiquitous in microfluidic devices, and is central to electrokinetic actuation of flow. Several chemical mechanisms can give rise to the spontaneous separation of charge between two phases [8]. The most relevant to microfluidics are ionization of surface groups and preferential adsorption of ions of one charge or the other.

2.1.1 Ionization of surface groups

Many microfluidic substrates behave as weak acids in aqueous solutions, owing to reactivities of surface groups, *e.g.*, amines, carboxylic acids, or oxides. Glass/silica microdevices are a particularly well-studied example of such a system, due to their ubiquity in devices used for CE and other analytical techniques [9]. In glass substrates, surface silanol groups can be deprotonated in aqueous solutions leaving a negative surface charge:

$$\mathrm{SiOH} \overset{K_a}{\rightleftharpoons} \mathrm{SiO^-} + \mathrm{H^+} \tag{1}$$

The pK_a for this reaction is approximately 4.7 [9]. In cases like this where protonation/deprotonation of surface groups is the origin of charge, the charge-determining ions are H^+ and OH^-, and the electrokinetic properties of the system are a strong function of pH [10].

2.1.2 Differences in affinity for ions between the solid and liquid phases

Differences in affinity between the liquid phase and the solid phase for particular ions lead to charge separation by (i) preferential adsorption of ions from an electrolyte solution onto the surface and/or (ii) preferential solution of ions from the crystal lattice of an ionic salt [8]. Many Nernstian surfaces exhibit mechanism (ii), leading to a surface potential that is well defined as a function of the salt concentration. Silver halides, such as AgI, are examples of Nernstian surfaces. Their surface potential, ζ, as a function of the silver ion concentration, $[Ag^+]$, is defined by

$$\zeta = \frac{k_B T}{ze} \ln \frac{[\mathrm{Ag^+}]}{[\mathrm{Ag^+}]_{\mathrm{pzc}}} \tag{2}$$

where k_B is Boltzmann's constant, T is the temperature in K, z is the valence of the ion ($z = 1$ for AgI), e is the elementary charge, and pzc refers to the point of zero charge. Equation (2) assumes that as the bulk activity of Ag^+ ions is altered, the activity of surface Ag^+ ions remains constant. Microfluidic devices are in general not made from Nernstian materials [6, 10], but Nernstian surfaces can be useful in studying electrokinetics, since their surface electrical potential boundary conditions are well-defined.

2.2 The electrical double layer

The net charge density at fluid-solid interfaces coincides with an electrical potential and ion distribution structure within the fluid known as the electrical double layer (EDL). The surface charge generates an electric field, which pulls oppositely charged ions (counterions) toward the surface, and pushes like charges (co-ions) away from it. Counterions preferentially concentrate near the surface, effectively shielding the bulk solution from the surface charge. The shielding layer is often referred to as the Debye layer, or the EDL. A schematic diagram of the EDL is shown in Fig. 1.

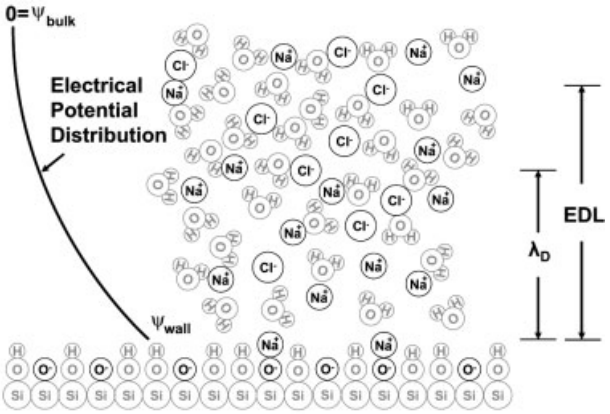

Figure 1. Scheme of the electrical double layer.

Detailed descriptions of the internal structure of the EDL are often based on the Gouy-Chapman-Stern (GCS) model [11], where the EDL is comprised of a Stern layer and a diffuse layer. The Stern layer consists of counterions which are immobilized on the surface, and its thickness is dictated by the size of the ions. The diffuse layer lies just beyond the Stern layer, and is responsible for the electrokinetic phenomena relevant to microfluidic devices.

For descriptions of electroosmosis in this context, it is sufficient to treat the diffuse layer ion distribution in the Boltzmann limit in which ions are treated as point particles in a mean field. The Poisson equation for the electric charge density, ρ_e, in a medium of electrical permittivity, ε, combined with the Boltzmann equation gives

$$\nabla^2 \psi = \frac{-\rho_e}{\varepsilon} = -\frac{1}{\varepsilon} \sum_i n_{0,i} e z_i \exp\left(-\frac{e z_i}{k_B T} \psi\right) \tag{3}$$

where ψ is the electrical potential, z_i is the valence of the i-th ionic species, and $n_{o,i}$ is the number density of the i-th species where $\psi = 0$. A natural length scale that arises in solutions of the Poisson-Boltzman equation is

$$\lambda_D = \sqrt{\frac{\varepsilon k_B T}{2e^2(\Gamma/2)}} \tag{4}$$

where λ_D, commonly referred to as the Debye length, is the length scale over which electrical potentials and ion distributions change and $\Gamma/2$ is the bulk ionic strength of the solution defined as:

$$\frac{\Gamma}{2} = \frac{1}{2}\sum_i n_{0,i} z_i^2 \tag{5}$$

Solution of the Poisson-Boltzmann equation is non-trivial due to its non-linearity and uncertainty in the boundary conditions. While Eq. (3) is usually sufficient for descriptions of macroscopically observable electrokinetic behavior in microdevices, the Boltzmann approximation breaks down at high electrolyte concentrations and in general fails to accurately describe ion distributions very close to the surface, where the ion size becomes important. Several, more sophisticated theories have led to versions of the Poisson-Boltzmann Equation modified to include the effects of ion size, use of the Ornstein-Zernike equation with hypernetted chain approximations [12, 13], and semi-empirical corrections based on mean spherical approximations [14] and Monte Carlo simulations [15].

2.3 Electrokinetic phenomena at solid-liquid interfaces in microfluidic devices

2.3.1 Electroosmosis

When an external electric field is applied to a fluid in a microchannel with an ion distribution described by Eq. (3), flow results. This phenomenon is termed electroosmosis. If the channel is straight and homogeneous with a uniform surface charge density, and its dimensions are large as compared to the Debye length, the flow profile is essentially uniform (Fig. 2a), and the bulk value of the fluid velocity is given by the Smoluchowski Equation. This stems from the assumptions that fluid properties are uniform and the no-slip boundary condition applies precisely at the "wall," at which $\psi = \zeta$.

$$u_{EO} = -\frac{\varepsilon\zeta}{\eta}E \tag{6}$$

where ζ is the electrokinetic potential, η is the fluid viscosity, and E is the applied electric field. In the Smoluchowski limit, then, the electroosmotic mobility, μ_{EO}, is given by

$$\mu_{EO} = -\frac{\varepsilon\zeta}{\eta} \tag{7}$$

The ζ potential is often inferred from measurements of μ_{EO} [6, 10, 16–20], but the precise meaning of ζ in relation to the electrical potential at the surface is in dispute [8, 21]. Here we phenomenologically define ζ from Eq. (7), and in simple models assume that ζ is equal to the difference in electrical potential between the bulk solution and the fluid-solid interface. Electroosmosis is commonly used to actuate flow in microfluidic channels, since it can dominate over pressure-driven flow at small length scales.

2.3.2 Streaming current and streaming potential

Pressure-driven flow in a microchannel results in the bulk motion of charges. When there is charge separation at the fluid-solid interface, this results in the net motion of unbalanced charge in the fluid, and therefore a net electrical current. In flow driven by a uniform pressure gradient, $\frac{\Delta P}{L}$, in a channel with circular cross-section and in the Debye-Hückel approximation ($e\zeta << k_B T$), the electrical current, called streaming current, is

$$I_{stream} = \frac{\varepsilon\zeta}{\eta}\frac{\Delta P}{L}A \tag{8}$$

where A is the cross-sectional area of the channel and $\Delta P = P_{downstream} - P_{upstream}$. While the streaming current given by Eq. (8) specifically applies to channels with circular cross-section, it is still a good approximation for other geometries in the limit where the double layers are thin compared to the channel height or radius and the flow is fully developed [10]. Similarly, if flow is driven by pressure but the current path is not closed (Fig. 2b), an electrical potential, $\Delta\phi$, called streaming potential, results.

$$\Delta\phi = \frac{\varepsilon\zeta}{\eta\sigma}\Delta P \tag{9}$$

Here σ is the conductivity of the fluid. Equation (9) also uses the Debye-Hückel approximation, and assumes the thin EDL limit so that channel geometry effects are unimportant. The conductivity is also assumed to be uniform throughout the channel, though in small channels the non-uniform ion distribution and surface conduction may have significant effects

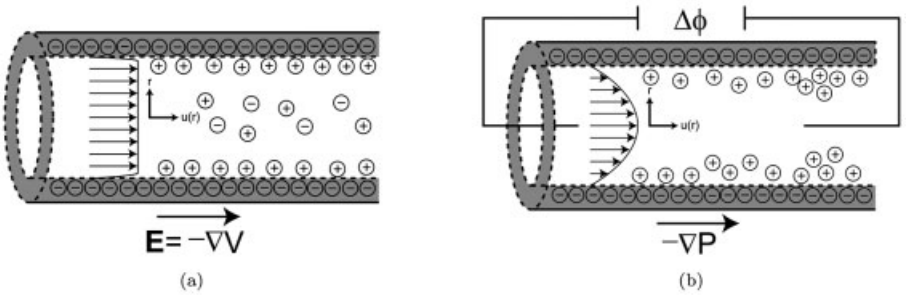

Figure 2. (a) Scheme of uniform electroosmotic flow resulting from an applied electric field. (b) Scheme of the redistribution of ions in pressure driven flow in a microchannel, resulting in a streaming potential. Ion sizes and distributions in the schematics are not to scale.

[22]. Streaming potential is often used as an alternative method for measuring the ζ potential [2, 23–25].

3 Materials and methods

3.1 Chemical reagents and solutions

All reagents were obtained from Sigma-Aldrich (St. Louis, MO) unless specified otherwise. Phosphate buffers were prepared from stock solutions of monobasic and dibasic potassium phosphate. Acetate buffers were prepared from sodium acetate and glacial acetic acid. Solution conductivity and pH were measured with a dual pH/conductivity meter (Mettler Toledo SevenMulti, Columbus, OH) with specialized electrodes (Mettler Toledo Inlab 730 and Inlab 413, Columbus, OH). Solution pH was adjusted by titration with sodium hydroxide and hydrochloric acid. Fluid viscosity was measured by monitoring the pressure drop of known laminar flow rates through microchannels of known fluidic resistance.

3.2 Polymer capillaries

PTFE capillaries were acquired from Scientific Commodities (Lake Havasu City, AZ). Zeonor® and TOPAS® capillaries were acquired from Paradigm optics (Vancouver, WA). PTFE, TOPAS®, and Zeonor® 1020R capillaries were used with inner/outer diameters of 330/762, 25/360, and 125/250 μm, respectively. Capillaries were equilibrated with solution for 8 h before testing.

3.3 Zeta potential measurement

Phase-sensitive streaming potential and automated current monitoring were used to measure the zeta potential in polymer microchannels. All experiments were run at room temperature ($T = 25°C$). For streaming potential, pressure (0-0.35 MPa) was applied to the inlet of the capillary using a push/pull syringe pump (KD Scientific, Holliston, MA). Sinusoidal pressure waveforms were established *via* syringe actuation combined with a PID controller corrected for the pressure-dependence of the system's pressure-displacement response. Control signals were implemented in LabView. Fluidic connections to the capillary, electrodes, and pressure transducer were made using 360 μm stainless-steel tubing and PEEK-ULTEM fittings (LabSmith, Livermore, CA) [26]. Platinized platinum electrodes connected to a 10 TΩ electrometer (6514 Electrometer, Keithley, Cleveland, OH) measured the generated voltage across the channel and a strain-gauge type transducer (Senso-Metrics SP70D, Simi Valley, CA) measured the pressure at the inlet. The forcing pressure and capillary diameters were chosen such that the flow was laminar (Reynolds number below 1200), surface conductivity was negligible, and errors due to hydrodynamic starting lengths could be ignored. The zeta potential was calculated using the Smoluchowski equation (Eq. 9). Errors introduced by the wall curvature and the use of Eq. (9) to describe non-Debye-Hückel charge distributions are ignored here since they are small as compared to temperature and conductivity uncertainties. Experiments were repeated a minimum of 20 times for each datum, and results are presented as the mean where error bars indicate the standard deviation.

For current monitoring [16, 27], 150-300V was applied across four 8 cm capillaries using an 8-channel high-voltage sequencer (LabSmith HVS448, Livermore, CA) and platinum electrodes. Control signals were implemented in LabView. Current was monitored on the four remaining channels, after extensively calibrating the device with known resistors. The reservoirs at each end used solutions with conductivities that varied by 5-7.5%. Square-wave voltage sequences were applied with period designed to allow electroosmosis to completely displace the fluid in the capillary during each half-cycle. The resulting current waveforms were fit to a trapezoidal profile and the shape was converted into a velocity measure. Joule heating and the attendant overprediction of electroosmotic mobility was eliminated by measuring the electroosmotic mobility as a function of applied field, and extrapolating to the zero-field limit. Only those electric fields that led to electrophoretic mobilities within 5% of the low-field limit were used. Pressure imbalances along the system were monitored during 8-hour test series and removed in postprocessing. The zeta potential was calculated using the Smoluchowski equation (Eq. 6). Errors introduced by the wall curvature are ignored here also since they are small as compared to temperature and conductivity uncertainties.

4 The origins of charge at water-hydrophobe interfaces

In Section 2, we provided a summary of standard equations and phenomena interpreted entirely from the standpoint of surfaces with well-understood surface charge formation mechanisms and no-slip boundary conditions, combined with assumptions that liquid properties such as viscosity and permittivity are uniform throughout and unaffected by (a) ion populations, (b) electric fields, and (c) short-range inter-molecular potentials associated with the surface. With these assumptions, the (i) governing equations (*i.e.* Poisson-Boltzmann equation), (ii) constitutive relations (*i.e.*, constant permittivity and viscosity), and (iii) boundary conditions are all reasonably well-defined. While these assumptions are mostly valid for hydrophilic surfaces, many of them are questionable or incorrect for hydrophobic substrates.

At water-hydrophobe interfaces, the origin of charge is not well-understood (electrostatic and chemical boundary conditions are not well-defined), there may be slip (the fluid velocity boundary conditions are not well-defined), and interfacial water structuring can lead to significant deviations from mean field approximations (the governing equations and constitutive relations are not well-defined). Thus

theoretical modeling and design of hydrophobic microfluidic devices is quite challenging, making careful experimentation with controlled input parameters crucial in this field. In the following and in the companion to this paper [1], we summarize and comment on the current state of experiments and modeling in this field, and provide recommendations for future studies.

The origins of surface charge in common hydrophobic microfluidic substrates are both (a) in dispute and (b) difficult to measure. Most hydrophobic materials are considered chemically inert, and are not expected to have reactive charge-forming surface groups or a strong affinity for ions. Nevertheless, several different hydrophobic materials, including PDMS, polystyrene (PS), polyethylene (PE), Zeonor®, and PTFE have been shown to have significant surface charge [6]. The hypotheses regarding the source(s) for charge include: (i) surface impurities are present owing to the manufacturing process; these undergo charge-forming chemical reactions when in contact with water; (ii) salt anions are specifically adsorbed, owing to differences in affinity or hydration energy; and (iii) hydroxyl ions are specifically adsorbed, owing to water orientation at a hydrophobic interface. These mechanisms and their relation to observed data are discussed in greater detail below.

4.1 Impurities

A common postulate for the origin of charge at polymer-water interfaces is that residual plasticizers, cross-linkers, and initiators from the manufacturing/polymerization process become functional surface groups capable of charge-forming chemical reactions, such as acid-base dissociation [18, 20, 28]. The prevalence of trade secrets in the polymer industry often leads to uncertainty as to the makeup and concentration of these impurities. We assess the possible role of impurities in interfacial charge for several common microfluidic materials in the following paragraphs.

PDMS is one of the most commonly used microfluidic substrates, owing to its relatively low cost, ease of fabrication, permeability, and elastomeric properties [3,4]. It has been shown that both native and oxidized PDMS exhibit electroosmotic flow, though the electroosmotic mobility of plasma-oxidized PDMS is larger and similar to that of glass [4, 20]. In [20], Ocvirk *et al.* found that μ_{EO} for native PDMS has a pH dependence very similar to that of fused silica capillaries, and that μ_{EO} did not change with the introduction of different electrolytes, unless high concentrations of large organic surfactants such as sodium dodecyl sulfate (SDS) were used. As a result, they concluded that "silica fillers" introduced by the manufacturer are the origin of charge in native PDMS. Ren *et al.* [28] also cited silica fillers as the putative origin of charge. However, their attenuated total reflection infrared (ATR-IR) spectroscopy experiments showed that oxygen plasma treated PDMS has large O-H stretches (which suggests the existence of silanol groups on the surface), while native PDMS does not; the absence of silanol spectroscopic features on native PDMS seems inconsistent with the hypothesis that silica filler impurities account for the surface charge. More recently, Wheeler *et al.* [29] also found that μ_{EO} in PDMS does not depend on the relative amount of curing agent used, indicating that impurities, if important, seem insensitive to concentration.

PTFE is less common as a microfluidic substrate, but is often used as a spun coating (usually in the form of Teflon® AF) to modify microfluidic channel surfaces to control contact angle or biocompatibility, especially in electrowetting-on-dieletric devices [30–33]. Data for μ_{EO} as a function of pH in PTFE (Fig. 3) shows very good agreement among different sources for pH values between 2 and 7, although there is a significant amount of scatter at high (> 7) pH [6, 17, 18, 23 25]. In Fig. 3, ζ is normalized by $pC = -\log C$, where C is the total counterion concentration in moles/liter. This representation stems from the engineering approximation $\zeta = a \log C$, proposed in [10] as a way to simplify representation of ζ-potential data for microfluidic substrates measured by multiple investigators. In order for impurities to be the origin of charge across the entire practical pH range, this agreement between data taken with different suppliers of PTFE manufactured with radically different methods, and with several different methods for measuring μ_{EO}, can only be explained if synthesis of PTFE produces similar impurities in all cases.

Olefins such as polystyrene (PS), polyethylene (PE), and poly(vinyl chloride) (PVC) were explored as substrates for microfluidics applications and analytical separations in the 1990s and the beginning of the 21st century [18, 19, 34–36]. More recently, cyclic olefin copolymers (COCs) such as Zeonor®, Zeonex®, and TOPAS® resins, have started to dominate use of olefins in microfluidics applications–owing to their good optical properties, high chemical resistance, and low water absorbance. Earlier work [18] on polymer capil-

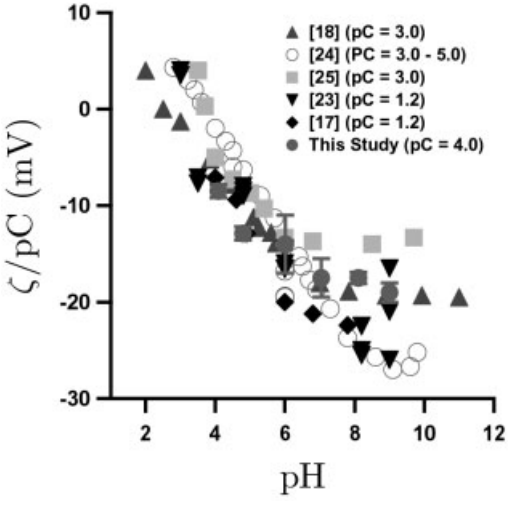

Figure 3. ζ normalized by pC (= – log C, C is the counterion concentration in M) as a function of pH for PTFE. Modified from [6] with addition of recent current monitoring data from the authors.

laries (PTFE, PE, PVC) observed sigmoidal pH dependence consistent with charged sites with p*K*a near 4.5, and postulated that carboxylic acids from impurities were responsible for the surface charge density. Mela *et al.* [2] have shown that μ_{EO} for Zeonor® resins exhibits sigmoidal pH dependence consistent with charged sites with $pK_a = 4.8$; here we report results with both current monitoring and streaming potential experiments that are consistent with those earlier results, despite using different laboratories, experimenters, fluidic platforms, and measurement techniques (Fig. 4a). Our streaming potential measurements of ζ as a function of pH in TOPAS® (Fig. 4b) showed very similar results, but simultaneously raise questions. Since the cyclopentadiene structure that dominates Zeonor® does not have any ionizable sites, one possible explanation for this behavior is the existence of carboxylic acid groups, which would arise from either oxidation of the cyclopentadiene structure or from the presence of proprietary plasticizers. However, Mela *et al.* showed both *via* XPS and *via* chemical functionalization that no significant amount of carboxylic acid surface moieties exist. At present, it seems unlikely that surface functional groups that have eluded detection *via* fluorescent and XPS techniques could be solely responsible for the electrokinetic behavior observed for these materials in contact with aqueous solutions.

While impurities certainly may affect the electrokinetic performance of some hydrophobic materials used in microsystems, impurities cannot explain the majority of the observed data. Many hydrophobic materials show consistent electrokinetic properties independent of the manufacturing process [6]. In fact, there is little, if any, support for the postulate that impurities are a primary source of charge in any polymeric microfluidic system. Relatively few experiments have been conducted to detect the role of impurities (a short summary of some is shown in Table 1), with minimal results.

4.2 Specific adsorption of (salt) ions

Specific adsorption of ions is known to affect many surfaces; for example, divalent cations, if present at high concentrations, have been shown to change the sign of the electrokinetic potential on glass surfaces at high pH [37]. While specific adsorption is often a minor issue for highly charged hydrophilic surfaces, the effect of adsorption of free ions from solution may become more important and easier to measure when the surface has few, if any, charged groups. In buffered electrolyte solutions, salt ions can lead to a net surface charge density if some ions are preferentially adsorbed over others owing to differences in their affinity or hydration energy [38, 39]. While adsorption is of course critical for large surfactant molecules, amphipathic surfactants are beyond the scope of the current work, and we focus here on small salt ions. In order for a hydrated ion to be able to adsorb to a surface, water molecules must be removed, so less-hydrated ions tend to preferentially adsorb as compared to more-hydrated ions. A summary of experiments testing for interfacial electrolyte anion adsorption is shown in Table 2.

A number of spectroscopic and molecular dynamics (MD) studies have provided direct evidence for the adsorption of electrolyte ions at liquid-gas interfaces [40–43], which serve as model hydrophobic interfaces owing to the well-defined geometry and the absence of hydrogen bonding in the gas phase. Sum frequency generation (SFG) measurements of air-water systems indicate enhanced anion concentration at the interface at high (> 0.1 M) salt concentrations [40, 41, 44, 45]. Recent XPS experiments performed at water-vapor interfaces with very high (saturated) salt concentrations demonstrated similar behavior [43]. Second harmonic generation (SHG) data for these interfaces across a range of salt concentrations (1 mM – 1 M) show that ion adsorption follows Langmuir adsorption kinetics [42]. This

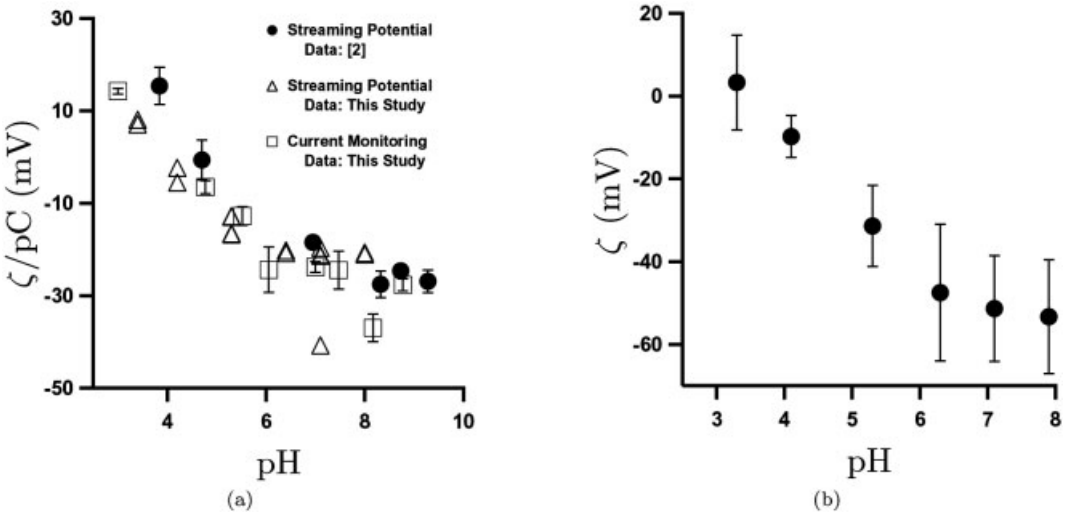

Figure 4. (a) ζ normalized by *pC*= – log *C* (*C* is the counterion concentration in M) as a function of pH for Zeonor®. (b) Streaming potential data showning ζ as a function of pH for TOPAS® (*pC* = 3)

Table 1. Summary of experiments with discussion of impurities

	Interface	Electrolytes used	Concentration ranges studied	Results
Schutzner [18]: μ_{E0} measurements	Water in PVC, PS, and PTFE microchannels	Betaine	10 mM	All materials had similar sigmoidal ζ *vs.* pH curves, with pK_a = 4.8. Surface carboxylate groups are postulated as the origin of charge, since the pK_a is similar to the value for aliphatic carboxylic acids.
Ocvirk [20]: Current monitoring	Water in oxidized and native PDMS microchannels	KCl, phosphate	11 mM	ζ-Potentials are larger in magnitude for oxidized compared to native PDMS. The ζ *vs.* pH behavior for oxidized PDMS is similar to that for glass.
Ren [28]: Current monitoring, ATR-IR	Water in oxidized and native PDMS microchannels	Phosphate	10 and 20 mM	ATR-IR shows that surface – OH groups in oxidized PDMS disappear over time with exposure to air. μ_{EP} for native PDMS is stable over time. μ_{EP} for oxidized PDMS is stable when the PDMS is stored in buffer, but unstable when it is exposed to air.
Mela [2]: Amine-function-alized dyes	Water in Zeonor® microchannels	Phosphate, acetate, Tris, borate	10 mM	Zeonor®surfaces incubated with amine-functionalized dyes showed no fluorescence, indicating that they did not have significant surface concentration of carboxylic acid groups.

Table 2. Summary of anion adsorption results

	Interface	Electrolytes used	Concentration ranges studied	Salt ion adsorption behavior
Franks [47]: μ_{EP} measurements	Hexadecane droplets in water	NaCl, NaBr, NaI, NaF, $NaClO_4$, $NaIO_3$, LiCl, CsCl	0.1 – 11 mM	No interfacial enhancement of salt anions; mobility changes with salt concentration are consistent with double layer shielding effects, independent of the ion type
Mela [2]: Streaming potential	Water in Zeonor® microchannels	Phosphate, acetate, Tris, borate	10 mM	ζ – Potential data taken with different electrolytes fit on the same sigmoidal curve
Petersen [42]: SHG	Air-water	NaN_3	10^{-3} – 1M	Enhanced N_3^- concentration at the interface, following Langmuir kinetics
Huang [46]: MD simulations	Solid-water: contact angle = 140° and 50°	NaI, NaCl	0.2 M and 1M	Interfacial enhancement of large ions, *i.e.* I^-
Liu [40]: SFG, Raman, ATR-FTIR	Air-water	NaCl, NaBr, NaI, NaF	0.820 M, 2.07 M	Enhanced Br^- and I concentrations at the interface
Vrbka [41]: MD simulations	Air-water	NaCl, NaBr, NaI, NaF	1.2M	Enhanced Br^- and I concentrations at the interface
Ghosal [43]: XPS	Vapor-liquid	KBr, KI	Saturated	Enhanced Br^- and I concentrations at the interface, more so for I^-

attraction of ions to vapor-liquid interfaces has been used to explain anomalous electrokinetic effects seen in molecular dynamics simulations of hydrophobic nanochannels, where both the existence of a region of depleted water density and specific ion concentration were seen [46].

While spectroscopic data provides clear evidence for salt ion adsorption at vapor-liquid interfaces in solutions with high salt concentration, data from electrokinetics experiments involving hydrophobic surfaces and lower salt concentrations (0.1 – 1 mM) does not conclusively support salt ion adsorption [2, 6, 47]. Measurements of electrophoretic mobility as a function of the counterion concentration have been shown to be explained by Gouy-Chapman-type double layer shielding effects and are in general independent of the particular buffer ions used for a variety of hydrophobic microfluidic substrates [2, 6]. The electrophoretic mobility of

oil droplets was also found to be buffer-independent, and scaled in a manner consistent with double layer shielding [47]. The discrepancy between the spectroscopic measurements taken at high salt concentrations and the electrokinetic measurements taken at low concentrations suggests there may be certain regimes of experimental parameters where salt ion adsorption becomes more or less important; certainly effects seen at high concentrations of large anions such as Br^- and I^- may not be significant for low concentrations of smaller ions such as Na^+ or Cl^-. At low salt concentrations, poor signal-to-noise ratio could hinder SFG/SHG experiments, which could explain the lack of spectroscopic evidence for salt adsorption in the < 1 mM regime. However, the data in [42], which covers a concentration range which is between those studied in microfluidics and other spectroscopic measurements (1 mM – 1 M), shows that the degree of interfacial salt adsorption decreases rapidly as the salt concentration is decreased. This suggests that at low concentrations, salt anion adsorption is also physically less important, and may be very difficult to observe in the presence of other chemical processes (*e.g.*, surface reactions or hydroxyl adsorption).

4.3 Specific adsorption of hydroxyl ions

The specific adsorption of hydroxyl ions onto hydrophobic interfaces has also been proposed as an origin of surface charge in microfluidic substrates [48, 49]. Even though hydroxyl ions tend to be more hydrated as compared to hydronium or salt ions [39], they are believed to preferentially adsorb onto aqueous-hydrophobic interfaces resulting in a net negative surface charge density [50]. This putative mechanism is analogous to the preferential adsorption of iodide at AgI crystal surfaces (Eq. 2), which leads to a *pzc* at pAg = 5.5 for AgI solutions at room temperature (see *e.g.* [51]). Molecular dynamics simulations have shown that structuring of water at the interface may facilitate this process [52, 53], which can be energetically favorable if hydroxyl ions hydrogen bond with ordered water molecules. This interfacial charging mechanism is consistent with experimental data for most hydrophobic surfaces, which have pH-dependent electrokinetic potentials that become increasingly negative with increasing pH [6]. However, simple models based solely on hydroxyl ion adsorption fail to explain positive charges on hydrophobic substrates [2], differences between different hydrophobic materials [18], and materials that have erratic behavior as a function of experimental parameters [6].

Interfacial charging by hydroxyl ion adsorption has been used to explain the electrokinetic behavior of oil droplets [47, 50, 54–56] and hydrophobic colloids [57] in aqueous electrolyte solutions (Table 3). Marinova *et al.* [50] studied the electrokinetic properties of oil droplets as a function of oil type, pH, and electrolyte concentration. They showed that xylene, dodecane, hexadecane, and perfluoromethyldecalin droplets all had nearly the same electrophoretic mobility, and that the electrolyte concentration dependence could be explained by compression of the double layer without specific salt ion adsorption. The pH dependence of μ_{EP} along with a hydroxyl ion adsorption model based on Stern isotherms gave a specific adsorption energy of 25 kT *per* ion. Later studies demonstrated similar behavior [55, 56], including some that specifically examined salt concentration dependence at relatively low salt concentrations (in the 0.1 – 11 mM concentration range) [47]. In an experiment with solid colloids, Ametov *et al.* [57] found a significant decrease in the ζ-potential when they increased the hydrophobicity of silica colloids by

Table 3. Summary of oil droplet/colloidal experiments in the context of hydroxyl ion adsorption

	Interface	Electrolytes used	Concentration ranges studied	Results
Dickinson [54]: μ_{EP} measurements	Octadecane and paraffin droplets in water	NaCl, phosphate, borate	0.01 N	All μ_{EP} vs. pH curves were similar, where μ_{EP} increases with increasing pH
Marinova [50]: μ_{EP} measurements	Xylene, dodecane, hexadecane and perfluoromethyldecalin droplets in water	NaCl, Na_2CO_3, urea	0.01 – 10 mM	The ζ-potential does not depend on the oil type, is increasingly negative with increasing pH, and is unaffected by addition of Na_2CO_3 up to 1 mM. Dependence on NaCl concentration is consistent with double layer compression
Ho [55]: Dynamic light scattering	Palm olein droplets in water	NaCl, $MgCl_2$, $CaCl_2$	1.5 mM, 0.15 mM	The ζ-potential is increasingly negative with increasing pH. Differences between monovalent and divalent ions are consistent with double layer shielding effects.
Graciaa [56]: Spinning tube zetameter	*n*-Alkane droplets in water (6 to 14 carbon atoms)	NaCl	10^{-4} – 10 mM	Alkane length has little effect on ζ-potential. Results agree with [50].
Ametov [57]: Phase analysis light scattering	Methylated silica colloids in water	KNO_3	1 mM	ζ-Potential is reduced for methylated silica spheres. The general shape of the ζ *vs.* pH curves is unaffected by methylation.

methylation. Though the magnitude of the ζ-potential was reduced, colloids with contact angle ~ 90° still showed pH-dependence that can be modeled by hydroxyl ion adsorption.

Some researchers studying solid-liquid interfaces in microfluidic systems have also postulated hydroxyl ion adsorption as the origin of charge [24, 48, 58]. Streaming potential measurements on plasma deposited fluorpolymer (PDFP) systems demonstrated significant changes in the ζ-potential with the addition of KOH or NaCl [24]. Werner *et al.* postulated that the changes were due to preferential adsorption of H_3O^+ and OH^- ions, owing to the fact that PDFP has no ionizable surface groups. Zimmermann *et al.* [48] observed similar behavior with Teflon® AF, and additionally postulated that preferential adsorption of H_3O^+ and OH^- ions is facilitated by hydrogen bonding with ordered water structures [50], a mechanism which has since gained support from molecular dynamics simulations [52, 53, 59]. The idea of stabilizing ordered water structures is also experimentally supported by SFG spectra of liquid vapor interfaces, which show characteristic peaks corresponding to dangling surface hydroxyl bonds and ice-like hydrogen-bonded hydroxyl groups. [45]. The structure of water at hydrophobic interfaces is of critical importance, and is discussed in greater detail in the companion to this paper [1].

5 Conclusions and recommendations

Identifying the origins of charge on hydrophobic surfaces is inherently challenging, owing to the added complexities of slip phenomena, uncertainties in interfacial structures, and unknown surface chemistry. While much of the microdevice and electrophoresis literature refers anecdotally to impurities as a source of charge, there are very few methodical studies of impurities in hydrophobic microfluidic substrates. At present, appreciable electrokinetic potentials can be observed on a variety of hydrophobic surfaces [6, 49], in a manner unexplained by postulated impurities and inconsistent with the lack of charged groups in the native material. The most direct studies of salt adsorption [47] indicate that salt ions are not appreciably adsorbed in a concentration range for which significant electrokinetic potentials are observed, thus making salt adsorption unsatisfactory for explaining many of the observed phenomena. Hydroxyl ion adsorption appears to be the most satisfactory explanation for the surface charge; however, this mechanism still lacks the comprehensive experimental and numerical validation required for general adoption. Beattie [49], for example, proposes hydroxyl ion adsorption as the source of charge on hydrophobic substrates owing to roughly consistent isolectric points (p*I*'s) observed on several materials combined with other supporting data. While many hydrophobic polymers do have similar p*I*'s, the differences between these p*I*'s are significant as compared to experimental uncertainty, and these differences are not fully explained by OH^- adsorption. Further, many materials for which OH^- adsorption is not presumed to play a significant role (*e.g.*, PC, PMMA, silica) have p*I*'s within the same range. At this point, the universality of OH^- adsorption as the source of charge on hydrophobic surfaces is promising, but yet to be demonstrated.

Experimentation in this area is challenging, owing to the large number of input parameters involved (*e.g.* pH, temperature, electrolyte ions, *etc.*), fluctuations in data due to transient or unstable chemical processes, and the coupling of slip with electrokinetic phenomena. Molecular dynamics simulations in this area are also challenging, owing to the complex nature of potentials for water and the inability of individual models to reproduce a wide variety of test parameters [60]. Further, the charge density expected on these surfaces is only moderate, and thus the spatial extent of the system required to achieve usable statistics requires an extensive calculation.

Future studies on the origin of charge in hydrophobic microfluidic devices should be focused on (i) bridging thermodynamic models with experimental data, and (ii) attempting to isolate the effects of each of the charge forming mechanisms independently through carefully designed experiments. Examination of the temperature dependence of these systems can lead to progress with the former, as chemical equilibria and ion distributions are both temperature-dependent. For the latter, there are several experiments which would lead to progress in this field, *e.g.*: (a) a methodical study of the effects of impurities, where impurities are implanted into a hydrophobic microfluidic substrate, and (b) electrokinetic characterization of hydrophobic substrates using solutions of high (> 0.1 M) salt concentration.

The authors have declared no conflict of interest.

6 References

[1] Tandon, V., Kirby, B. J., *Electrophoresis* 2007, *28*, this issue.

[2] Mela, P., van den Berg, A., Fintschenko, Y., Cummings, E. B., *et al.*, *Electrophoresis* 2005, *26*, 1792–1799.

[3] Stone, H. A., Stroock, A. D., Ajdari, A., *Ann. Rev. Fluid Mech.* 2004, *36*, 381–411.

[4] McDonald, J. C., Duffy, D. C., Anderson, J. R., Chiu, D. T., *et al.*, *Electrophoresis* 2000, *21*, 27–40.

[5] Hawkins, B. G., Smith, A. E., Syed, Y. A., Kirby, B. J., *Anal. Chem.* 2007, *79*, 7291–7300.

[6] Kirby, B. J., Hasselbrink, E. F., *Electrophoresis* 2004, *25*, 203–213.

[7] Lauga, E., Brenner, M. P., Stone, H. A. (Eds.) *Handbook of Experimental Fluid Dynamics*. Springer, New York 2005.

[8] Hunter, R. J., *Zeta Potential in Colloid Science*, Academic Press, London 1981.

[9] Iler, R. K., *The Chemistry of Silica*, Wiley, New York 1979.

[10] Kirby, B. J., Hasselbrink, E. F., *Electrophoresis* 2004, *25*, 203–213.

[11] Hunter, R. J., *Foundations of Colloid Science, Vol. 2*, Clarendon Press, Oxford 1989.

[12] Attard, P., *Phys. Rev. E* 1993, *48(5)*, 3604–3621.

[13] Attard, P., *Adv. in Chem. Phys.* 1996, *92*, 1–159.

[14] Fawcett, W. R., Henderson, D. J., *J. Phys. Chem. B* 2000, *104*, 6837–6842.

[15] Boda, D., Henderson, D., Plaschko, P., Fawcett, W. R., *Molecular Simulation* 2004, *30*, 137–140.

[16] Huang, X., Gordon, M. J., Zare, R. N., *Anal. Chem.* 1988, *60*, 1837–1838.

[17] Lukacs, K. D., Jorgenson, J. W., *J. High Resolut. Chromatogr.* 1985, *8*, 407–411.

[18] Schutzner, W., Kenndler, E., *Anal. Chem.* 1992, *64*, 1991–1995.

[19] Locascio, L. E., Perso, C. E., Lee, C. S., *J. Chromatogr. A* 1999, *857*, 275–284.

[20] Ocvirk, G., Munroe, M., Tang, T., Oleschuk, R., *et al.*. *Electrophoresis* 2000, *21*, 107–115.

[21] Lyklema, J., *Fundamentals of Interface and Colloid Sci.*, *Volume II: Solid-Liquid Interfaces*, Academic Press, London 1995.

[22] Lyklema, J., Minor, M., *Colloids Surfaces A* 1998, *140*, 33–40.

[23] Reijenga, J. C., Aben, G. V. A., Verheggen, T. P. E. M., Everaerts, F. M., *J. High Resolut. Chromatogr.* 1983, *8*, 407–411.

[24] Werner, C., Korber, H., Zimmermann, R., Dukhin, S., Jacobasch, H., *J. Colloid Interface Sci.* 1998, *208(1)*, 329–346.

[25] Lappan, U., Buchhammer, H.-M., Lunkwitz, K., *Polymer* 1999, *40*, 4087–4091.

[26] Kirby, B. J., Reichmuth, D. S., Renzi, R. F., Shepodd, T. J., Wiedenman, B. J., *Lab Chip* 2005, *5*, 184–190.

[27] Ross, D., Locascio, L. E., *Anal. Chem.* 2003, *75*, 1218–1220.

[28] Ren, X., Bachman, M., Sims, C., Li, G. P., Allbritton, N., *J. Chromatogr. B* 2001, *762*, 117–125.

[29] Wheeler, A. R., Trapp, G., Trapp, O., Zare, R. N., *Electrophoresis* 2004, *25*, 1120–1124.

[30] Moon, H., Cho, S. K., Garrell, R. L., Kim, C.-J., *J. Appl. Phys.* 2002, *92*, 4080–4087.

[31] Lee, J., Moon, H., Fowler, J., Schoellhammer, T., Kim., C.-J., *Sens. Actuators A* 2002, *95*, 259–268.

[32] Jones, T. B., Fowler, J. D., Chang, Y. S., Kim, C.-J., *Langmuir* 2003, *19*, 7646–7651.

[33] Cho, S. K., Moon, H., Kim, C.-J., *J. Microelectromech. Syst.* 2003, *12(1)*, 70–80.

[34] Voight, A., Wolf, H., Lauckner, H., Neumann, G., *et al.*, *Biomaterials* 1983, *4*, 299–304.

[35] Roberts, M. A., Rossier, J. S., Bercier, P., Girault, H., *Anal. Chem.* 1997, *69*, 2035–2042.

[36] Johnson, T. J., Ross, R., Locascio, L. E., *Anal. Chem.* 2002, *74*, 45–51.

[37] Gaudin, A. M., Fursteneau, D. W., *Trans. ASME* 1955, *202*, 66–72.

[38] Lyklema, J., *Fundamentals of Interface and Colloid Sci., Volume I: Fundamentals*, Academic Press, London 1991.

[39] Israelachvili, J. N., *Intermolecular and Surface Forces*, Academic Press, London 1992.

[40] Liu, D., Ma, G., Levering, L.M., Allen, H.C., *J. Phys. Chem. B* 2004, *108*, 2252–2260.

[41] Vrbka, L., Mucha, M., Minofar, B., Jungwirth, P., *Curr. Opin. Colloid Interface Sci.* 2004, *9*, 67.

[42] Petersen, P. B., Saykally, R. J., *Chem. Phys. Lett.* 2004, *397*, 51–55.

[43] Ghosal, S., Hemminger, J. C., Bluhm, H., Mun, B. S., *et al.*, *Sci.* 2005, *307*, 563–566.

[44] Baldelli, S., Schnitzer, C., Schultz, M., Campbell, D. J., *Chem. Phys. Lett.* 1998, *287*, 143–147.

[45] Raduge, C., Pflumio, V., Shen, Y. R., *Chem. Phys. Lett.* 1997, *274(1)*, 140–144.

[46] Huang, D. M., Cottin-Bizonne, C., Ybert, C., Bocquet, L., *Phys. Rev. Lett.* 2007, *98*, 177801.

[47] Franks, G. V., Djerdjev, A. M., Beattie, J. K., *Langmuir* 2005, *21*, 8670–8674.

[48] Zimmermann, R., Dukhin, S., Werner, C., *J. Phys. Chem. B* 2001, *105*, 8544–8549.

[49] Beattie, J. K., *Lab Chip* 2006, *6*, 1409–1411.

[50] Marinova, K. G., Alargova, R. G., Denkov, N. D., Velev, O. D., *et al.*, *Langmuir* 1996, *12*, 2045–2051.

[51] Larson, I., Attard, P., *J. Colloid Interface Sci.* 2000, *227*, 152–163.

[52] Dang, L. X., Chang, T., *J. Phys. Chem. B* 2002, *106*, 235–238.

[53] Mamatkulov, S. I., Khabibullaev, P. K., Netz, R. R., *Langmuir* 2004, *20*, 4756–4763.

[54] Dickinson, W., *Trans. Faraday Soc.* 1941, *37*, 140.

[55] Ho, C. C., Ahmad, K., *J. Colloid Interface Sci.* 1999, *216*, 25–33.

[56] Graciaa, A., Creux, P., Dicharry, C., Lachaise, J., *J. Dispersion Sci. Technol.* 2002, *23*, 301–307.

[57] Ametov, I., Prestidge, C. A., *J. Phys. Chem. B* 2004, *108(32)*, 12116–12122.

[58] Schweiss, R., Welzel, P., Knoll, W., Werner, C., *Chem. Commun.* 2005, *2*, 256–258.

[59] Zangi, R., Engberts, J. B. F. N., *J. Am. Chem. Soc.* 2005, *127*, 2272–2276.

[60] Guillot, B., *J. Mol. Liquids* 2002, *101*, 219–260.

